The n_TOF Total Absorption Calorimeter for neutron capture measurements at CERN

C. Guerrero [a,*], U. Abbondanno [b], G. Aerts [c], H. Álvarez [d], F. Álvarez-Velarde [a], S. Andriamonje [c],
J. Andrzejewski [e], P. Assimakopoulos [f], L. Audouin [g], G. Badurek [h], P. Baumann [g], F. Bečvář [i], E. Berthoumieux [c],
F. Calviño [j], M. Calviani [k], D. Cano-Ott [a], R. Capote [m,ae], C. Carrapiço [c,ag], P. Cennini [l], V. Chepel [n], E. Chiaveri [l],
N. Colonna [o], G. Cortes [j], A. Couture [p], J. Cox [p], M. Dahlfors [l], S. David [g], I. Dillmann [q], C. Domingo-Pardo [r],
W. Dridi [c], I. Duran [d], C. Eleftheriadis [s], L. Ferrant [g], A. Ferrari [l], R. Ferreira-Marques [n], K. Fujii [b], W. Furman [t],
I. Goncalves [n], E. González-Romero [a], F. Gramegna [k], F. Gunsing [c], B. Haas [g], R. Haight [u], M. Heil [v],
A. Herrera-Martinez [l], M. Igashira [w], E. Jericha [h], F. Käppeler [v], Y. Kadi [l], D. Karadimos [f], M. Kerveno [g], P. Koehler [x],
E. Kossionides [y], M. Krtička [i], C. Lampoudis [c,s], H. Leeb [h], A. Lindote [n], I. Lopes [n], S. Lozano [ae], S. Lukic [g],
J. Marganiec [e], S. Marrone [o], T. Martínez [a], C. Massimi [z], P. Mastinu [k], E. Mendoza [a], A. Mengoni [l,m], P.M. Milazzo [b],
C. Moreau [b], M. Mosconi [v], F. Neves [n], H. Oberhummer [h], S. O'Brien [p], J. Pancin [c], C. Papachristodoulou [f],
C. Papadopoulos [aa], C. Paradela [d], N. Patronis [f], A. Pavlik [ab], P. Pavlopoulos [ac], L. Perrot [c], M.T. Pigni [h], R. Plag [v],
A. Plompen [ad], A. Plukis [c], A. Poch [j], J. Praena [k], C. Pretel [j], J. Quesada [ae], T. Rauscher [af], R. Reifarth [u], C. Rubbia [l],
G. Rudolf [g], P. Rullhusen [ad], J. Salgado [ag], C. Santos [ag], L. Sarchiapone [l], I. Savvidis [s], C. Stephan [g], G. Tagliente [o],
J.L. Tain [r], L. Tassan-Got [g], L. Tavora [ag], R. Terlizzi [o], G. Vannini [z], P. Vaz [ag], A. Ventura [ah], D. Villamarin [a],
M.C. Vicente [a], V. Vlachoudis [l], R. Vlastou [aa], F. Voss [v], S. Walter [v], M. Wiescher [p], K. Wisshak [v]

[a] Centro de Investigaciones Energeticas Medioambientales y Tecnologicas, Madrid, Spain
[b] Istituto Nazionale di Fisica Nucleare, Trieste, Italy
[c] CEA/Saclay – DSM/DAPNIA, Gif-sur-Yvette, France
[d] Universidade de Santiago de Compostela, Spain
[e] University of Lodz, Lodz, Poland
[f] University of Ioannina, Greece
[g] Centre National de la Recherche Scientifique/IN2P3-IReS, Strasbourg, France
[h] Atominstitut der Österreichischen Universitäten, Technische Universität Wien, Austria
[i] Charles University, Prague, Czech Republic
[j] Universidad Politecnica de Catalunya, Spain
[k] Istituto Nazionale di Fisica Nucleare (INFN), Laboratori Nazionali di Legnaro, Italy
[l] CERN, Geneva, Switzerland
[m] International Atomic Energy Agency (IAEA), Nuclear Data Section, Vienna, Austria
[n] LIP – Coimbra and Departamento de Fisica da Universidade de Coimbra, Portugal
[o] Istituto Nazionale di Fisica Nucleare, Bari, Italy
[p] University of Notre Dame, Notre Dame, USA
[q] Physik-Department E12, Technische Universität München, Garching, Germany
[r] Instituto de Física Corpuscular, CSIC-Universidad de Valencia, Spain
[s] Aristotle University of Thessaloniki, Greece
[t] Joint Institute for Nuclear Research, Frank Laboratory of Neutron Physics, Dubna, Russia
[u] Los Alamos National Laboratory, NM, USA
[v] Forschungszentrum Karlsruhe GmbH (FZK), Institut für Kernphysik, Germany
[w] Tokyo Institute of Technology, Japan
[x] Oak Ridge National Laboratory, Physics Division, Oak Ridge, USA
[y] NCSR, Athens, Greece
[z] Dipartimento di Fisica, Università di Bologna, and Sezione INFN di Bologna, Italy
[aa] National Technical University of Athens, Greece
[ab] Institut für Isotopenforschung und Kernphysik, Universität Wien, Austria
[ac] Pôle Universitaire Léonard de Vinci, Paris La Défense, France
[ad] CEC-JRC-IRMM, Geel, Belgium
[ae] Universidad de Sevilla, Spain
[af] Department of Physics - University of Basel, Switzerland
[ag] Instituto Tecnológico e Nuclear(ITN), Lisbon, Portugal
[ah] ENEA, Bologna, Italy

* Corresponding author. Tel.: +34 913466778; fax: +34 913466576.
E-mail address: carlos.guerrero@ciemat.es (C. Guerrero).

ABSTRACT

The n_TOF Collaboration has built and commissioned a high-performance detector for (n, γ) measurements called the Total Absorption Calorimeter (TAC). The TAC was especially designed for measuring neutron capture cross-sections of low-mass and/or radioactive samples with the accuracy required for nuclear technology and stellar nucleosynthesis. We present a detailed description of the TAC and discuss its overall performance in terms of energy and time resolution, background discrimination, detection efficiency and neutron sensitivity.

1. Introduction

The Total Absorption Calorimeter (TAC) is a segmented 4π detector array made of 40 BaF_2 crystals for neutron capture cross-section measurements at the CERN n_TOF Neutron Time-of-Flight Facility [1]. The high-efficiency detector in combination with long flight path of 185 m and high instantaneous neutron flux at n_TOF of 1.2×10^6 neutrons/pulse provides the opportunity for accurate neutron capture cross-section measurements on low-mass and/or radioactive samples for applications in nuclear technology [2–4] and stellar nucleosynthesis [5,6]. In the specific fields of accelerator driven systems (ADS) for transmutation of nuclear waste and of Generation-IV reactors, the need for more accurate cross-sections has been widely discussed [7], and many n_TOF measurements have already been funded by EC Framework Programs (n_TOF-NDADS [8], IP-EUROTRANS [9]) and other international projects.

At n_TOF, neutron capture cross-sections are measured using either a pair of C_6D_6 total energy detectors or the TAC. The first technique is based on low-efficiency, low-energy resolution detectors with an efficiency proportional to γ-ray energy [10]. The current version consists of C_6D_6 detectors, for which the required proportionality with γ-ray energy is achieved by the pulse height weighting technique [11,12]. This technique is also used for neutron capture measurements at GELINA [13], ORELA [14], and KURRI [15].

In contrast, the TAC is designed to detect the complete γ-ray cascade emitted in neutron capture reactions using detectors of high-intrinsic efficiency and large solid-angle coverage. By segmentation of the detector, the measured multiplicity can be combined with the deposited energy of a capture event for an improved background discrimination and for obtaining information on nuclear structure data characteristic of the compound nucleus [16].

The Total Absorption technique is best suited for measuring radioactive and/or small mass samples because of its high efficiency and background rejection capabilities. Large arrays of inorganic scintillators have therefore been built in the recent years for measuring neutron capture cross-sections, not only at n_TOF (40 BaF_2 crystals [17]), but also at other facilities such as FZK (41 BaF_2 crystals [27]), KURRI (4π Ge [18] and 16 BGO crystals [19]), RPI (16 NaI crystals [20]) and LANL (162 BaF_2 crystals [21]).

In this work we describe the n_TOF TAC and discuss its overall performance in terms of energy and time resolution, background, detection efficiency and neutron sensitivity. The detector, the associated data acquisition system, and the samples for the first applications of the TAC are described in Section 2. Test measurements with γ-ray sources are presented in Section 3, and the performance in the first measurements of (n, γ) cross-sections of ^{197}Au and ^{237}Np is discussed in Section 4, with particular emphasis on efficiency (Section 5) and neutron sensitivity (Section 6).

2. Experimental set-up

2.1. The n_TOF facility

At the n_TOF facility [1] neutrons are generated in spallation reactions by a pulsed 20 GeV proton beam impinging on a lead block, which is surrounded by 5 cm of water which serves as a coolant and as a moderator of the originally fast neutron spectrum. The resulting white neutron beam ranges from thermal energies to over 250 MeV with a nearly $1/E$ isolethargic flux dependence up to 100 keV. The neutrons travel through an evacuated beam line to the experimental area at a distance of 185.015(10) m from the spallation target. The intensity of the neutron beam in the experimental area is monitored by the *SiMon* system [22], an assembly of four silicon detectors facing a thin ^6Li foil which intersects the neutron beam.

The experimental program at n_TOF includes measurements of fission cross-sections performed with Parallel Plate Avalanche Counters (PPAC) [23] and a Fast Induction Chamber (FIC) [24] and of capture cross-sections studied either with total energy detectors (C_6D_6) [25] or with the TAC described in this paper.

An overview of the n_TOF facility and the various measuring devices is given in Ref. [26] and further details can be found in Ref. [1].

2.2. The Total Absorption Calorimeter

The n_TOF TAC is based on the BaF_2 calorimeter built at Forschungszentrum Karlsruhe [27] and was designed to meet the requirements of an ideal Total Absorption detector: large solid angle coverage, high total γ-ray efficiency, good energy resolution, high segmentation, low neutron sensitivity and fast time response.

The TAC consists of 40 BaF_2 crystals, 12 pentagonal and 28 hexagonal in shape, which cover 95% of 4π. Both types of crystals are cut from BaF_2 cylinders 1 cm in diameter and 15 cm thickness with raw and final weights of 12 and 7.5 kg, respectively. For optimal light collection each crystal is covered with two layers of 0.1 mm thick Teflon foil and a 0.1 mm thick polished aluminum sheet on the outside. The crystals are put into 1 mm thick ^{10}B loaded capsules and are coupled to an aluminum cylinder that houses also the 12.7 cm Photonis XP4508B photomultiplier. These individual detector modules are attached to an aluminum honeycomb structure, which holds the complete assembly. The TAC is divided into hemispheres that can be moved to open the detector for access to the samples in the center. Fig. 1 shows a picture of the open TAC with the neutron absorber surrounding the samples. Details of design, construction, and assembling of the TAC can be found in Ref. [28].

One of the main sources of background in (n, γ) measurements with the TAC is related to the capture of neutrons scattered in the
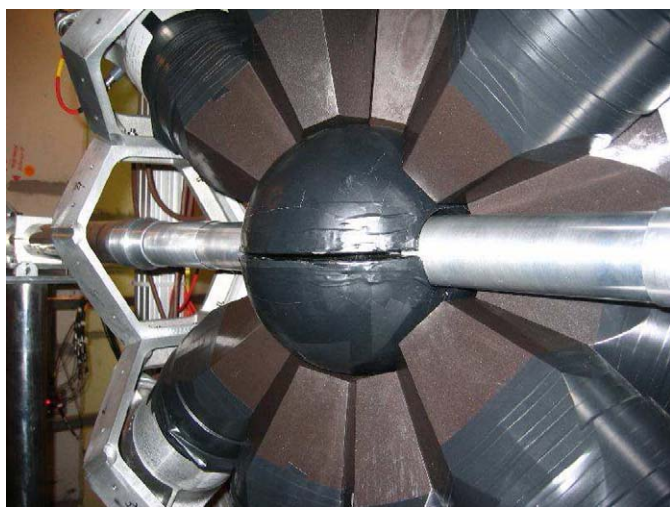
Fig. 1. View of one of the TAC hemispheres with the neutron absorber in the center and the neutron beam line.

Fig. 2. Sketch of the sample assembly including titanium can and Kapton frame.

sample. This background follows the same energy dependence as the true capture events and may therefore jeopardize the analysis of resonances. The probability for detecting such background events is referred to as the neutron sensitivity of the system. In the case of the TAC, this was reduced by combining the spherical neutron moderator/absorber surrounding the sample with the ^{10}B loaded (16% in mass) carbon fiber capsules of the crystals.

The neutron absorber material was selected by Monte Carlo simulations [30,29], which confirmed that the best neutron moderator/absorber combination is ^{6}LiH [21], which has the additional advantage of a very low γ-ray interaction cross-section thanks to its low effective atomic number Z. However, safety rules at CERN prohibit the use of ^{6}LiH due to its high flammability and toxicity, and therefore an inert non-flammable lithium salt $C_{12}H_{20}O_4(^6L)_2$ [29] was used instead. For stability, the compound was encapsulated in a spherical 0.5 mm thick aluminum shell with inner and outer radii of 5 and 10 cm, respectively. The absorber inside the TAC is shown in Fig. 1.

2.3. Samples

The samples used in a first series of TAC measurements were disks 1 cm in diameter. Stable samples were sandwiched between two Kapton foils and mounted in air between thin Kapton windows in the beam line. Radioactive samples had to be certified according to the ISO-2919 norm and were therefore sandwiched between two aluminum layers (<75 mg) and welded into titanium cans ($\sim$410 mg), as sketched in Fig. 2.

The data reported in this work refer to the TAC response to γ-rays from radioactive sources (^{137}Cs, ^{60}Co, ^{88}Y and ^{24}Na) and to (n, γ) reaction studies with stable (^{197}Au, graphite, and empty) samples; and with a radioactive (^{237}Np) sample. The measurements with the stable samples were performed to determine the ambient background (dummy-sample), the detection efficiency (^{197}Au), and the neutron sensitivity (graphite) of the TAC.

2.4. Data acquisition system

One of the main features of the experimental set-up at n_TOF is the fully digitized data acquisition system, which is described in detail in Ref. [31]. In particular, the BaF$_2$ signals are recorded by
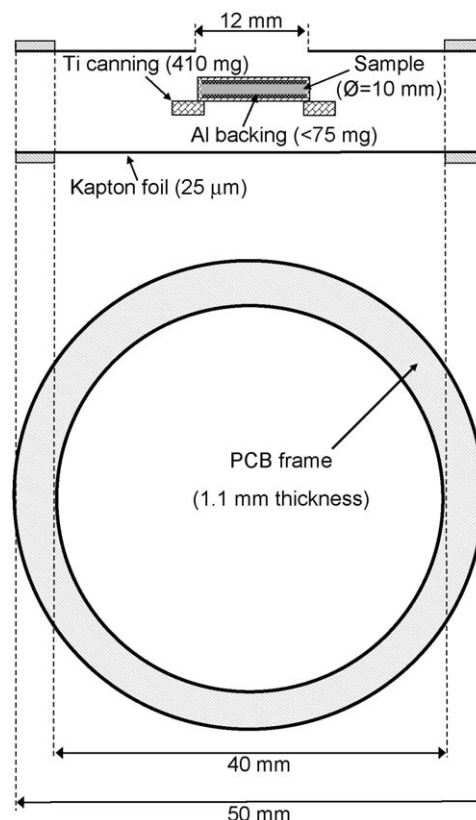
40 channels of high performance digitizers (Acqiris-DC270 [32]) with 8 bits resolution, 8 MB memory, and 500 MHz sampling rate. This system can record 16 ms long data buffers containing the digitized electronic response of each BaF$_2$ module for neutron energies between 0.3 eV and 20 GeV. A reduction in the sampling rate to 100 MSamples/s allows one to reach the $1/v$ energy region down to 0.028 eV.

After zero suppression and data formatting, the raw data are sent to CERN's massive CASTOR storage facility [33] via several Gigabit links. The raw data are stored in a temporary disk pool for on-line analysis and on magnetic tapes for repeated processing, thus providing the possibility for repeated investigations of systematic effects related to pile-up, γ/α discrimination, etc.

The digitized buffers are analyzed using a dedicated pulse shape analysis (PSA) routine for BaF$_2$ signals [34] that characterizes each signal by an analytic fit of the two components in the scintillation light ($\tau_{fast} = 0.7$ ns and $\tau_{slow} = 630$ ns). Fig. 3 shows an example of a digitized buffer containing five signals that are identified and reconstructed by the PSA routine.

The PSA routine extracts the relevant signal parameters for later data analysis, the Time-of-Flight (TOF), signal integral, and module identification number. This information is stored in data summary tapes, which are subsequently translated by coincidence analysis software into a list of detected events with a given neutron energy (E_n) calculated from the TOF, total deposited energy (E_{sum}) derived from the signal integral, and crystal multiplicity (m_{cr}) given by the number of modules involved in the detection of a capture of an event.

The existence of radium impurities in the crystals is responsible for a sizable α and β decay background that has been characterized experimentally (see Section 4.1). Signals produced by α-particles can be identified by the PSA routine because the

relative contributions of the fast and slow component of the light output depend strongly on the ionizing particle.

2.5. Measuring technique

By the TOF technique neutron cross-sections can be measured as a function of neutron energy. The technique is based on a pulsed neutron source, where the energy of the neutron inducing a detected reaction is determined by

$$E_n(eV) = \left(\frac{72.2996 \cdot L(m)}{t_{det}(\mu s) - t_0(\mu s)} \right)^2 \qquad (1)$$

where L is the distance between source and sample, and t_0 and t_{det} are the production and detection times, respectively. Note that this expression neglects relativistic effects and is, therefore, valid only below about 1 MeV.

Neutron capture reactions produce a cascade of several γ-rays with a total energy of $E_{casc} = S_n + (A/(A+1))E_n$, where A is the mass number of the isotope under study, S_n the neutron separation energy of the product nucleus, and E_n the energy of the incident neutron. The TAC is designed to absorb this cascade completely with efficiency as independent as possible from the decay scheme of the compound nucleus.

The observable quantity in (n, γ) measurements is the capture yield $Y_{n,\gamma}(E_n)$, which is the fraction of neutrons intersecting the sample undergoing a capture reaction. Experimentally, it is defined as

$$Y_{n,\gamma}(E_n) = \frac{C(E_n) - B(E_n)}{\varepsilon_{n,\gamma} N \Phi_n(E_n)}, \qquad (2)$$

where $C(E_n)$ and $B(E_n)$ are the total and background count rates, $\varepsilon_{n,\gamma}$ the detection efficiency for capture cascades, $\phi_n(E_n)$ the intensity of incident neutrons recorded by the *SiMon* system, and N the proportionality constant between the neutron intensity incident on the *SiMon* ($\oslash = 3$ cm) and on the sample ($\oslash = 1$ cm). For the purpose of this work, $N = 0.191(6)$ was calculated from the characterization of the neutron beam profile [43] and the
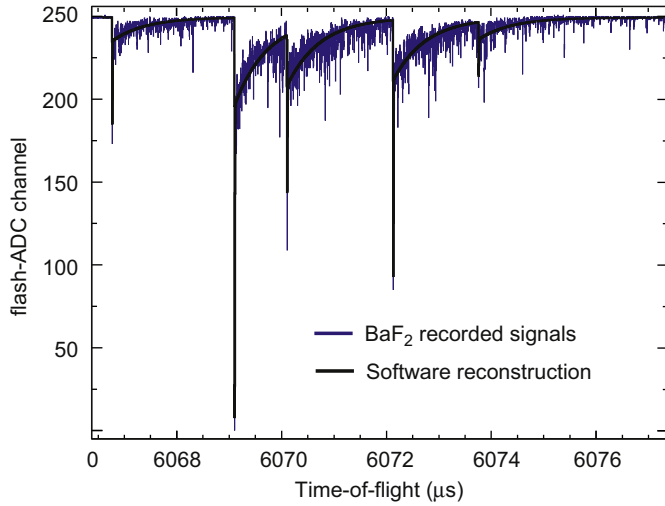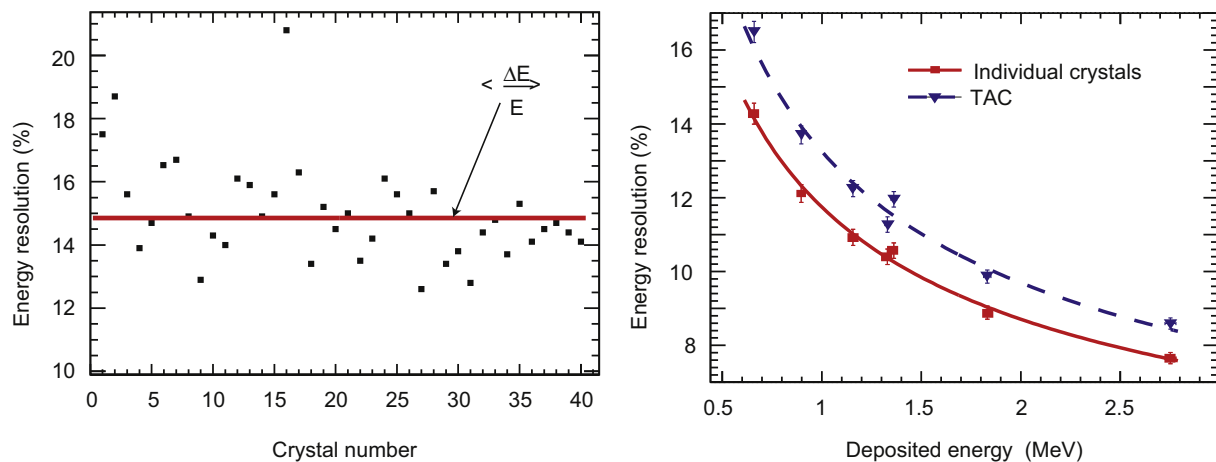

Fig. 3. Digitized buffer containing five BaF$_2$ signals that are identified and reconstructed by the PSA routine.
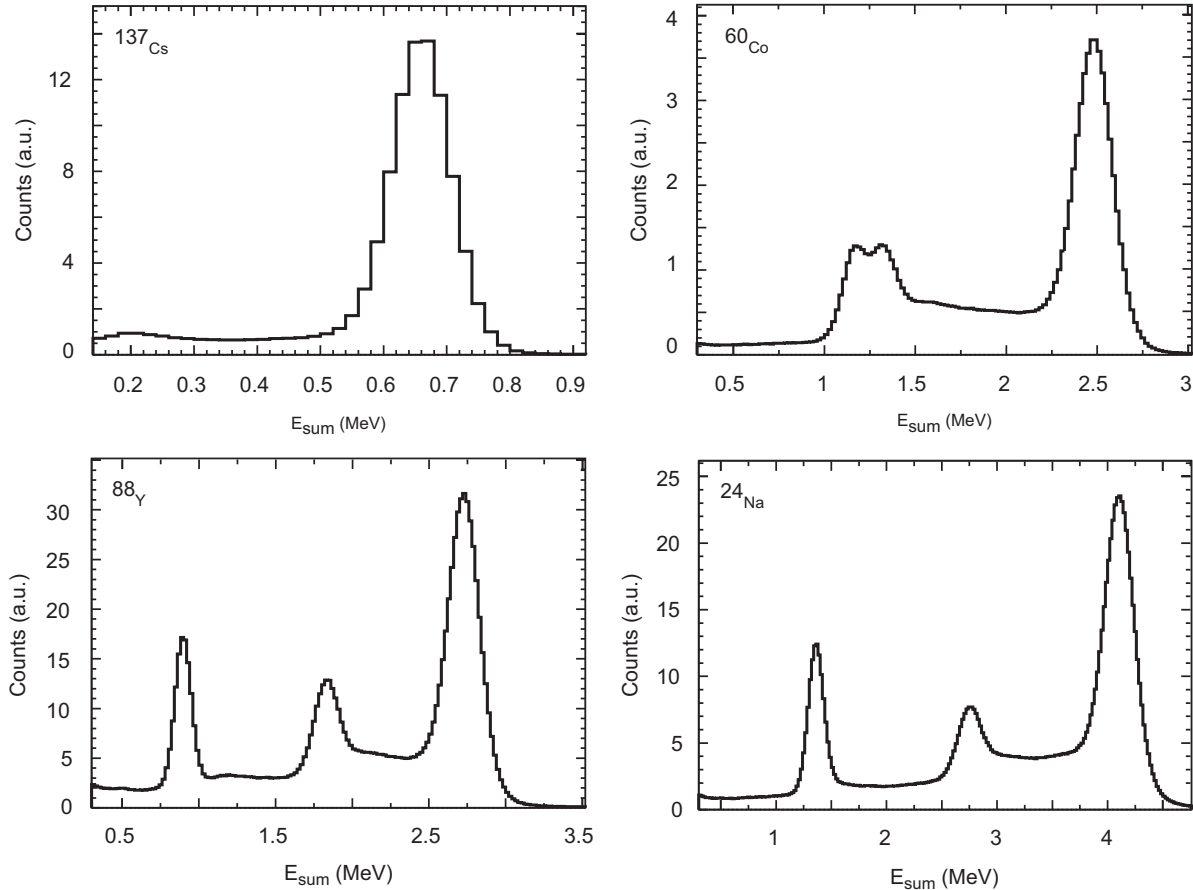
Fig. 4. TAC response to the standard γ-ray sources ^{137}Cs, ^{60}Co, ^{88}Y and ^{24}Na.

Fig. 5. Left: energy resolution of the individual modules at the energy of the ^{137}Cs peak (662 keV). Right: energy resolution averaged over the individual modules (squares) and of the complete TAC (triangles). The lines correspond to fits of the data with the expected energy dependence.

distance between the *SiMon* and the sample, although it can be determined experimentally in each individual measurement.

3. Detector performance

3.1. Energy calibration and resolution

The energy response of each individual BaF$_2$ module was characterized by standard γ-ray sources, i.e. ^{137}Cs, ^{60}Co, ^{88}Y, and ^{24}Na as illustrated by the examples in Fig. 4. The energy resolution per crystal measured with the ^{137}Cs source is plotted in the left panel of Fig. 5. The distribution exhibits a spread of about 2% around a mean energy resolution of ∼15% due to variations in the quality of the crystals and of the photomultipliers.

The energy resolution of the complete detector assembly is shown in the right panel of Fig. 5. The mean values measured with the available calibration sources are indicated by squares and the solid line is a fit of the data with the expected energy dependence. The energy resolution of the complete TAC is slightly worse due to the scatter in the resolution and the uncertainty in the energy calibration of the individual crystals.

The energy calibration of the TAC is based on weekly calibration measurements with γ-ray sources up to the energy of a ^{238}Pu/^{13}C source of 6.1 MeV. The daily variation in the gain of each module is monitored by the position of the α lines of radium and its progeny [27]. The α spectrum for a single module is shown in Fig. 6, where the peak used for gain monitoring is highlighted.

3.2. Time resolution

With the fast component in the scintillation light of $\tau_{fast} =$ 0.7 ns a time resolution of better than 1 ns can be achieved for each individual module [27]. Coincidence measurements, however, require a wider time window to be defined for collecting the signals from all γ-rays of a given capture cascade. This is due to the time that elapses until all γ-rays are absorbed, and mainly due to the 2 ppm uncertainty in the synchronization of all flash-ADC channels [32].

The width of the coincidence window has been set to 20 ns, which was found to be required for reconstructing the complete cascades emitted by the calibration sources. The length of the coincidence window does not affect the TOF resolution, which is
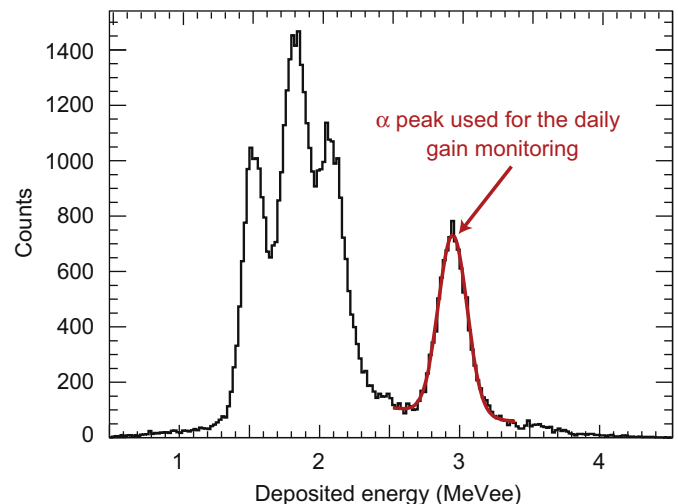
Fig. 6. The α spectrum of a single module. The peak used for monitoring time variations in gain is highlighted.

dominated by the resolution function associated with the neutron production and moderation processes [1,37].

4. Measurements

In the following, we present the first measurements performed with the TAC with emphasis in the different type of background observed. The test measurements were made with

- a ^{197}Au sample of 185 mg, which has been used as a reference in previous works [39,13,40];
- a ^{237}Np sample of 43 mg, which was the first radioactive sample measured with the TAC [35];
- a natural carbon sample of 70 mg, which served as a pure scatterer.

4.1. Background

Each of the backgrounds in (n, γ) measurements with the TAC produces a characteristic response in terms of energy and

multiplicity, which can be classified according to their correlation with the neutron beam.

Backgrounds that are not correlated with the neutron beam are mainly due to the γ-ray activity of the radioactive samples with energies up to a few hundred keV, and to the radium impurities in the BaF_2 crystals with α and γ-ray energies up to a few MeV [27]. These backgrounds are characterized experimentally by dedicated *beam-off* measurements.

Backgrounds correlated with the neutron beam depend on neutron energy and also on the neutron capture and scattering cross-sections of the materials involved. These are mainly

- cascades from (n, γ) reactions in the sample canning and in beam line windows, and
- capture of neutrons scattered in the sample; taking the capture place in the neutron absorber, the ^{10}B-loaded capsules, or in the Ba and F isotopes of the crystals.
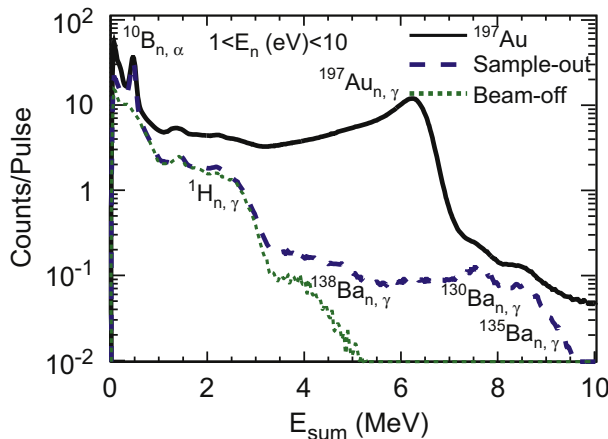
These backgrounds have been characterized in dedicated runs. While the uncorrelated part was measured in *sample-out* runs, the backgrounds due to capture and scattering reactions in the sample assembly were determined in runs with a *dummy-sample* and with the *carbon scatterer*.

A last type of background that is dominant in measurement with Total Energy detectors at n_TOF, the in-beam γ-rays of 2.2 MeV caused by neutrons absorbed in the water moderator surrounding the spallation target, is just a negligible low energy background in the case of the TAC due to its high Total Absorption efficiency for capture cascades.

4.2. The reference case of ^{197}Au

The magnitude of background contributions is illustrated in the case of a real experiment with the 185 mg ^{197}Au sample. The comparison in Figs. 7 and 8 refers the measured deposited energy distributions in two energy intervals and the TOF spectrum between 1 eV and 30 keV. Such an upper limit corresponds to the energy above which the γ-flash of relativistic particles coming with the beam has a significant saturation effect on the electronics. The experimental distributions are normalized to the neutron beam intensity determined by the *SiMon* system in units of nominal proton pulses.

Fig. 7 shows the distributions of the deposited energy in the TAC (E_{sum}) for energy intervals from 1 to 10 eV (left) and from 1 to 10 keV (right). The contribution from capture reactions in ^{197}Au is limited to ~7.0 MeV, just above the neutron separation energy at $S_n(^{198}Au) = 6.54$ MeV; given that the summing of events due to pile-up is negligible. The main difference in the two E_n intervals is the magnitude of the background with respect to the capture reactions in ^{197}Au due to the relative energy dependency of the capture and scattering cross-sections of the indicated isotopes.

At low deposited energy, the *beam-off* measurement shows three components related to the β^- decay of radium and its progeny in the BaF_2 crystals [27]. The ^{226}Ra decay chain yields a contribution of up to 3.2 MeV, while the ^{228}Ra contribution ranges from 2.2 (^{212}Bi decay) to 5.0 MeV (^{208}Tl decay). The peak at 1.46 MeV corresponds to ambient ^{40}K. The background from scattered neutrons along the beam line is characterized by the sample out measurement, which shows a peak at 0.478 MeV from the decay of $^7Li^*$ produced by (n, α) reactions in the ^{10}B loaded capsules, a small structure at 2.2 MeV from $^1H(n, \gamma)$ reactions in the neutron absorber, and a high energy contribution from 4.7 to 9.1 MeV due to neutron captures in Ba and F. Events with deposited energies above 9.5 MeV indicate pile-up due to events overlapping within the 20 ns coincidence window.

Fig. 8 shows the TOF spectrum obtained in the three dedicated runs discussed before. The events were selected corresponding to
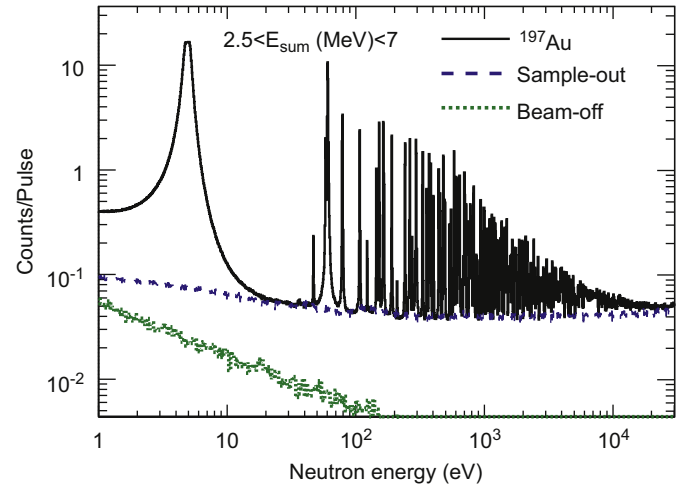
Fig. 8. Count rate distribution obtained with the ^{197}Au sample and backgrounds measured in dedicated runs with and without a dummy sample. Events were selected for deposited energies between 2.5 and 7 MeV, where the capture to background ratio is more favorable.
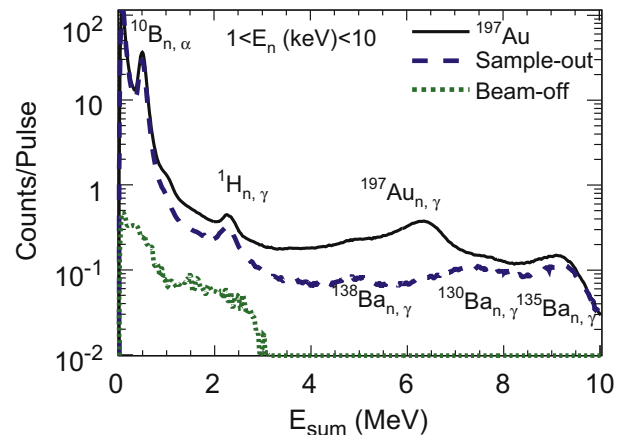
Fig. 7. Deposited energy distributions obtained with the 185 mg ^{197}Au sample and the related backgrounds in the neutron energy intervals from 1 to 10 eV (left) and from 1 to 10 keV (right).

deposited energies between 2.5 and 7 MeV, where the capture to background ratio is more favorable. The resonant structures of the ^{197}Au(n, γ) cross-section are observed well above the overall background and could be resolved up to several keV.

Due to the narrowing of the TOF bins, the background from radioactive impurities in the BaF$_2$ and the ambient background in the experimental area decreases with increasing energy and becomes negligible above a few tens of eV. The sample out run reveals a smooth background close to the ^{197}Au spectrum in the valleys between resonances and above a few tens of keV.

4.3. The ^{237}Np measurement

In measurements on radioactive samples, additional backgrounds are caused by the activity of the sample and by capture and scattering reactions in the titanium and aluminum components in the sample assembly.

This is illustrated in Fig. 9, which shows the E_{sum} distribution measured with the ^{237}Np sample of 43 mg and the various background contributions measured in dedicated runs. At energies below 0.5 MeV the spectrum is dominated by the γ-ray activity of the sample and at high energies by capture and scattering in the titanium canning.

In the neutron energy interval between 1 and 10 eV, this background is determined by capture reactions in ^{48,49,50}Ti. At higher neutron energies the Ti related background clearly exceeds the signal from and capture reactions in ^{237}Np, partly because of the comparably massive titanium can and partly because of the large resonant cross-sections in the keV region. This becomes obvious in Fig. 10 for neutron energies above a few keV. Nevertheless, the resonant structure of the ^{237}Np cross-section is observed with good signal/noise ratio up to about 1 keV.

It can be concluded that neutron capture cross-sections can be successfully measured with the TAC at least up to ~30 keV. However, this range is reduced to a few keV if the sample had to be encapsulated in titanium. This limitation can be overcome by using an alternative assembly for radioactive samples [38].

4.4. Neutron scattering background

Background from neutron scattering in the sample is of special concern because it follows the same resonant pattern as the capture reactions. In the past, this type of background was found to be responsible for significant systematic uncertainties in cases
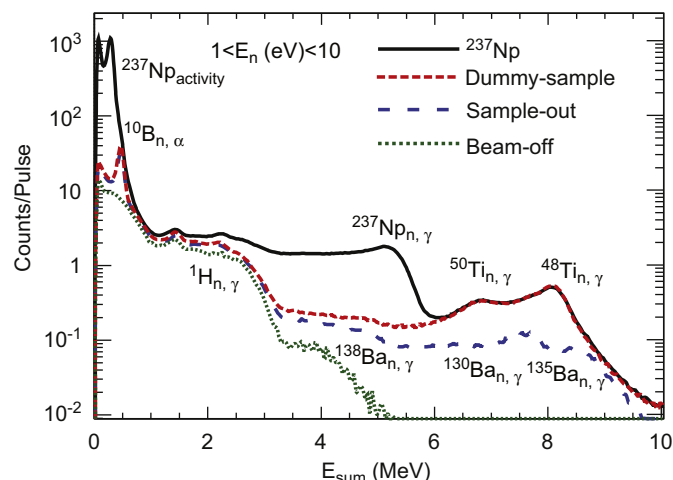

Fig. 10. Count rate distributions measured with the ^{237}Np sample and in dedicated backgrounds runs for deposited energies between 2.5 and 6 MeV.

where the scattering channel was much stronger than that for capture [47,40,13].

There are at least three ways of determining the scattering background:

1. Analytically, by taking the theoretical probability for scattering in the sample, the kinematics of neutron scattering, the distance traveled by the neutron between the sample and the detector, and the neutron sensitivity as a function of neutron energy into account. This analytical approach is implemented in the REFIT code for resonance analysis [48].
2. A similar calculation was proposed by Allen et al. [49] using Monte Carlo techniques instead of the analytical approach to describe the neutron scattering reactions and the related background.
3. The Total Absorption technique makes it possible to determine the background due to scattered neutrons experimentally as a function of neutron energy by comparison of the deposited energy distribution with that of a pure carbon scatterer [50], where $\sigma_n > 10^4 \sigma_\gamma$.

In our analysis we use the third method in order to rely only on experimental data and not on Monte Carlo neutron transport codes or multiple scattering models.

The TAC response to a graphite sample of 70 mg for neutron energies between 10 and 100 keV is shown in Fig. 11, where the structures are related to neutron capture reactions in the different isotopes present in the set-up. This pure neutron scattering spectrum is used to obtain a background-free capture spectrum as demonstrated in Fig. 12. The deposited energy distribution of the ^{197}Au sample—for the condition $m_{cr} > 2$ and after subtraction of the background components not related to sample scattered neutrons—can be decomposed into the scattering background and the true ^{198}Au (n, γ) events. The background component is obtained by normalizing the pure neutron scattering spectrum in the high energy region ($E_{sum} > 8.5$ MeV) above the neutron separation energy of gold.

This procedure is applied to the E_{sum} spectra for narrow E_n bins, resulting in a background-free capture spectrum as a function of neutron energy.

4.5. Conditions on crystal multiplicity and deposited energy

One of the main advantages of the Total Absorption technique is the possibility for background rejection by applying specific conditions with respect to crystal multiplicity (m_{cr}) and deposited energy (E_{sum}).

Fig. 9. Deposited energy distributions measured with the ^{237}Np sample and in dedicated background runs in the neutron energy interval between 1 and 10 eV.
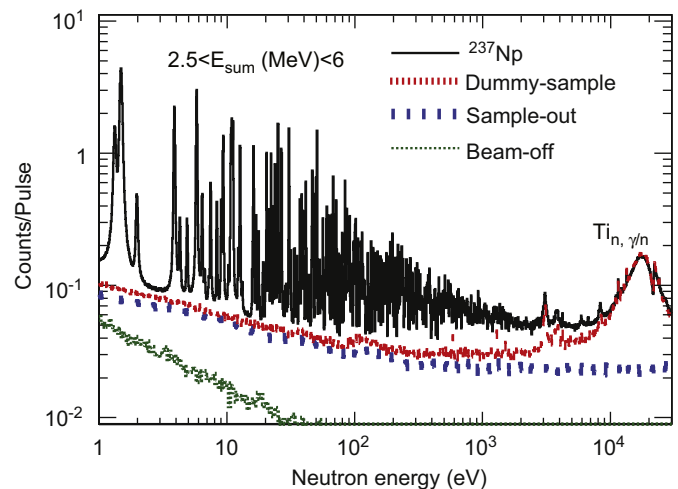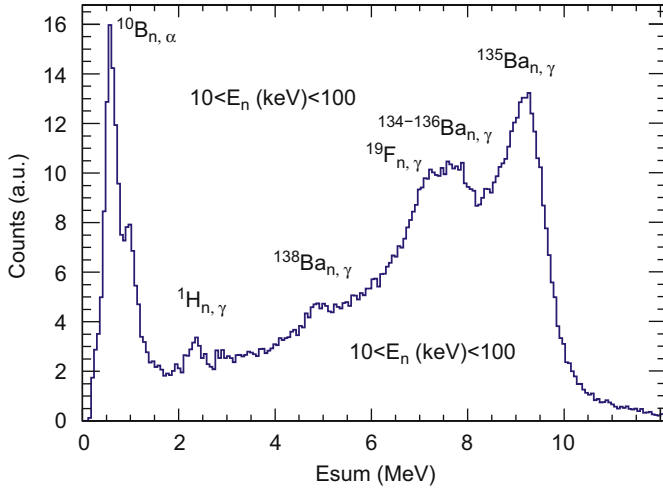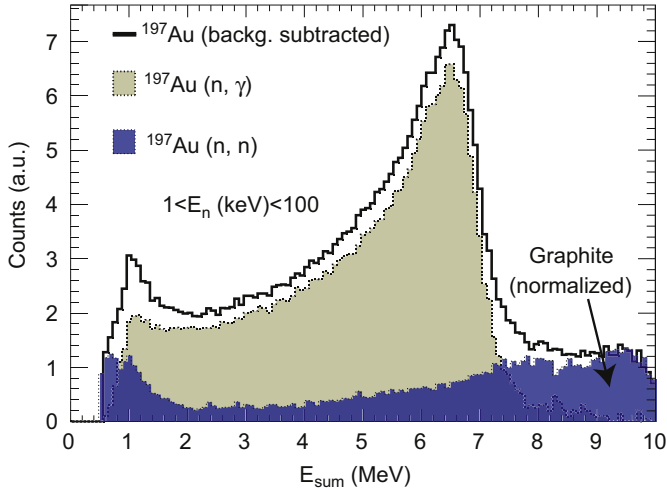
Fig. 11. Deposited energy distribution measured with a graphite sample for neutron energies between 10 and 100 keV.

Fig. 13. Deposited energy distribution from the $^{197}Au(n,\gamma)$ measurement for different crystal multiplicities in the neutron energy interval from 1 to 10 eV.
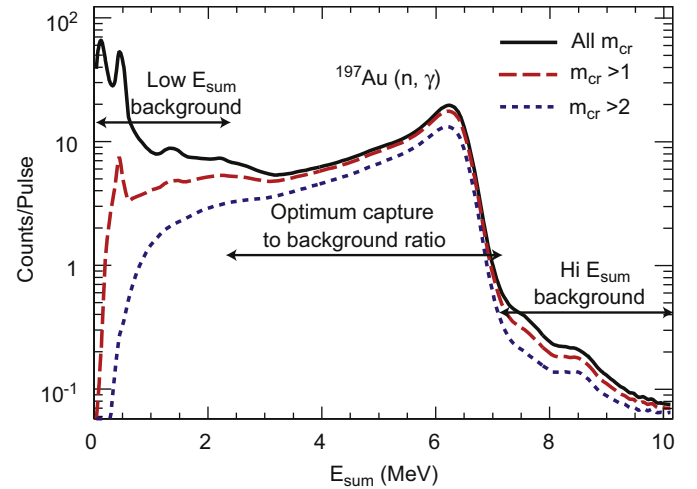

Fig. 12. Measured deposited energy distribution of ^{197}Au, separated into pure capture and scattering contributions for neutron energies between 1 and 100 keV and for the condition $m_{cr} > 2$.

The background reduction achieved by the m_{cr} condition is given in Fig. 13 for the $^{197}Au(n,\gamma)$ measurement. The three spectra shown correspond to the conditions $m_{cr} > 0$, $m_{cr} > 1$ and $m_{cr} > 2$. The low-energy background caused by the intrinsic γ-ray activity of the BaF_2 crystals and the 478 keV γ-ray following $^{10}B(n,\gamma)$ reactions is strongly reduced with $m_{cr} > 1$ and nearly eliminated with $m_{cr} > 2$. The background at the high-energy end of the spectrum, which is not much affected by either one of these conditions, can be eliminated by selecting an upper deposited energy threshold at 7 MeV.

The m_{cr} and E_{sum} conditions for the optimal capture to background ratio depend on the particularities of each measurement, e.g. on the radioactivity of the sample, the capture-to-scattering ratio, and the energy and average multiplicity of the capture cascades. For ^{197}Au, the best balance between background reduction and loss of efficiency was found for $m_{cr} > 2$ and $2.5 < E_{sum}(MeV) < 7$.

5. Detection efficiency

In principle, the large solid angle coverage and the 15 cm thick BaF_2 crystals result in a detection efficiency for capture events of

almost 100%, regardless of the de-excitation pattern of the compound system under study. However, the efficiency of the TAC is reduced by the neutron absorber as well as by the conditions set for m_{cr} and E_{sum}. At high counting rates it is further affected by pile-up events as outlined in Ref. [36].

The detection efficiency can be determined experimentally for any condition on m_{cr} and E_{sum} by means of the saturated resonance method [39], where the theoretical and the observed capture yields are compared for a particular resonance that meets the following requirements:

1. The peak cross-section and the sample thickness must be large enough for the resonance to be saturated at the top: $(1 - e^{-n\sigma_{tot}}) \to 1$.
2. The capture to scattering cross-section ratio must be large enough so that the saturation point ($Y_{n,\gamma}^{sat} \sim \sigma_\gamma / \sigma_\gamma + \sigma_n$) can be determined accurately.

For this purpose we used the well-known resonance of ^{197}Au at 4.9 eV [39].

The theoretical capture yield of ^{197}Au in the vicinity of the 4.9 eV resonance was calculated with the SAMMY code [41], assuming the resonance parameters of the JEFF-3.1 cross-section library [42], i.e. $\Gamma_\gamma = 122.5$ meV and $\Gamma_n = 15.2$ meV. The SAMMY calculation includes all known experimental effects such as self-shielding, multiple-scattering, Doppler and resolution broadening. The observed capture yield

$$Y_{n,\gamma}^{obs}(E_n) = \frac{C(E_n) - B(E_n)}{N \cdot \Phi_n(E_n)} \tag{3}$$

is derived from measured quantities, which have already been defined in Eq. (2).

The ^{197}Au capture yields with the saturated region between 4.7 and 5.1 eV are shown in Fig. 14 for different conditions. The lines are the theoretical yields scaled to match the experimental yields. The detection efficiency of the TAC for capture reactions on ^{197}Au is given by the respective scaling factor.

The detection efficiencies obtained in this way are listed in Table 1. Obviously, efficiency is reduced as the conditions become more restrictive. The quoted uncertainties are only determined by the accuracy of the SAMMY fit ($<1\%$), the saturation level of the resonance calculated with the evaluated cross-section from the
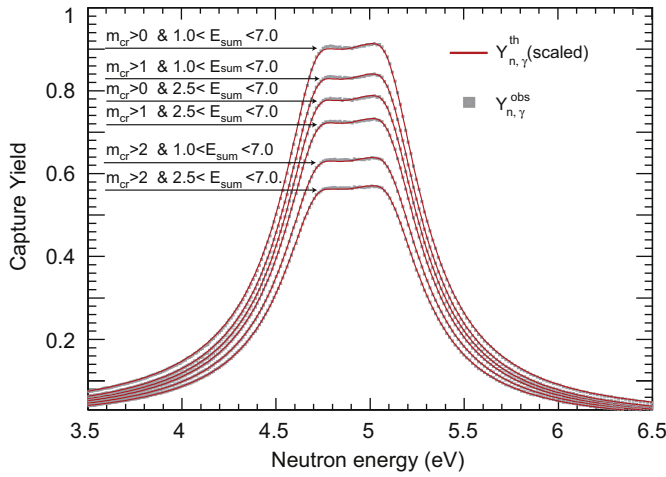
Fig. 14. Observed (symbols) and theoretical (lines) capture yields around the 4.9 eV resonance in ^{197}Au for different analysis conditions (E_{sum} in MeV). The detection efficiency of the TAC is obtained by scaling the theoretical yields to match the measured data.

Table 1
Detection efficiency of the TAC for ^{197}Au(n,γ) reactions under different analysis conditions.

	All m_{cr}	$m_{cr} > 1$	$m_{cr} > 2$
$1.0 < E_{sum}$ (MeV) < 7.0	0.91(5)	0.85(5)	0.64(3)
$2.5 < E_{sum}$ (MeV) < 7.0	0.79(4)	0.74(4)	0.58(3)

JEFF-3.1 library (2% [44]), and the incident neutron intensity $N\Phi_n$ (5% [1]).

An alternative technique for obtaining the detection efficiency is by Monte Carlo simulations with theoretically generated γ-ray cascades. This provides better accuracy in the determination of $\varepsilon_{(n,\gamma)}$ and can also be used in the absence of saturated resonances. Such Monte Carlo simulations have already been presented [45], but will be discussed in detail and applied to the n_TOF TAC in a forthcoming publication [46], where it is shown that the results agree within uncertainties with those of the saturated resonance method.
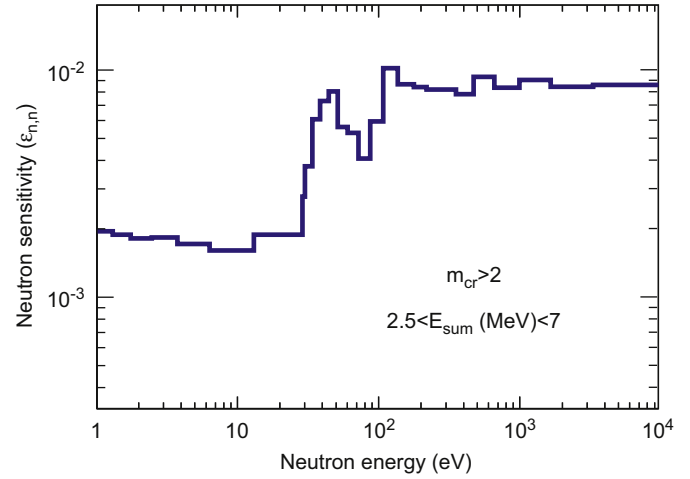
6. Neutron sensitivity

The neutron sensitivity of a detection system ($\varepsilon_{n,n}$) is defined as its efficiency for events induced by sample scattered neutrons. It is usually minimized in neutron capture measurements by avoiding materials with large capture cross-sections in the detector assembly and by a neutron shield between sample and detector. In the particular case of the TAC, a neutron moderator/absorber with a high ^{1}H and ^{6}Li content has been inserted in the central cavity and the crystal are mounted in ^{10}B loaded capsules.

The neutron sensitivity of the TAC has been obtained as a function of neutron energy from the spectra taken with the carbon sample by comparison with theoretically calculated neutron scattering yields

$$Y_{n,n}^{th} = (1 - e^{-n\sigma_{tot}})\frac{\sigma_n}{\sigma_{tot}} \qquad (4)$$

where the total (σ_{tot}) and scattering (σ_n) neutron cross-sections have been adopted from the JEFF-3.1 library [42]. The observed yields are

$$Y_{n,n}^{obs} = \frac{C - B}{N \cdot \Phi_n} \qquad (5)$$

Fig. 15. The neutron sensitivity of the TAC, $\varepsilon_{n,n}$, is derived from the yield measured with a carbon sample relative to a theoretical yield calculated from the scattering cross-section of ^{12}C.

where C and B are the total counting rate and the background of the run with the carbon sample measurement. In both equations, all but n, the number of atoms per barn, and N, the fraction of the beam seen by the sample, are neutron energy dependent variables.

The $\varepsilon_{n,n}$ found in this way are shown in Fig. 15. It varies as a function of neutron energy from 0.2% in the lower eV region up to about 1% above 100 eV. The sudden increase near 30 eV is related to neutron capture resonances in the Ba and F isotopes of the scintillator, which are also responsible for the structures around 40 and 100 eV.

Since the neutron sensitivity is approximately 100 times lower than the efficiency for detecting capture cascades, the background due to sample scattered neutrons becomes sizable ($> 1\%$) when $\sigma_n \geq \sigma_\gamma$.

7. Conclusions

The Total Absorption Calorimeter (TAC) of the n_TOF Collaboration has been described in some detail and the overall performance was studied with standard γ-ray sources as well as in dedicated TOF measurements with stable and radioactive samples.

The TAC exhibits a good capture to background ratio that can be further improved by imposing conditions on the deposited energy and multiplicity of the detected events. The neutron sensitivity $\varepsilon_{n,n}$ of the TAC has been measured and found to be less than 1% over the energy range between 1 eV and 10 keV. For the reference case of ^{197}Au, the detection efficiency for capture events, $\varepsilon_{n,\gamma}$, and its dependence on conditions concerning the deposited energy and multiplicity, has been determined experimentally by the saturated resonance method. It was found that $\varepsilon_{n,\gamma}$ remains as high as 58% even if rather restrictive conditions are imposed for background reduction (Table 1).

These results have confirmed that the TAC is a powerful tool for measuring neutron capture cross-sections of small and/or radioactive samples with high capture to background ratios and high detection efficiency.

References

[1] The n_TOF Collaboration, CERN n_TOF facility: performance report, CERN/INTC-O-011, INTC-2002-037 CERN-SL-2002-053 ECT, 2006.
[2] W. Gudowski, Nucl. Phys. A 654 (1999).
[3] G. Aliberti, et al., Nucl. Sci. Eng. 146 (2004) 13.
[4] J. Bouchard, Nuclear data for innovative reactors and fuel cycles, in: Proceedings of the International Conference on Nuclear Data for Science and Technology, vol. 718, Nice, France, 2007.
[5] G. Wallerstein, et al., Rev. Mod. Phys. 69 (1997) 995.
[6] M. Arnould, From the microcosm of the atomic nuclei to the macrocosm of the stars, in: Proceedings of the International Conference on Nuclear Data for Science and Technology, vol. 712, Nice, France, 2007.
[7] NEA/WPEC-26, Uncertainty and target accuracy assessment for innovative systems using recent covariance evaluations, ISBN 978-92-64-99053-1, 2008.
[8] http://www.cern.ch/n_TOF/n_TOF-ND-ADS/⟩.
[9] IP-EUROTRANS: European Research Program for Transmutation of High Level Nuclear Waste in Accelerator Driven Systems, FIGW-CT-2004-516520 nuklear-server.ka.fzk.de/eurotrans⟩.
[10] M.C. Moxon, E.R. Rae, Nucl. Instr. and Meth. A 24 (1963) 445.
[11] R.L. Macklin, J.H. Gibbons, Phys. Rev. 159 (1967) 1007.
[12] J.L. Tain, et al., J. Nucl. Sci. Tech. 689 (Suppl. 2) (2002).
[13] A. Borella, et al., Nucl. Instr. and Meth. A 577 (2007) 626.
[14] http://www.phy.ornl.gov/nuclear/orela/⟩.
[15] N. Yamamuro, T. Doi, T. Miyagawa, Y. Fujita, K. Kobayashi, R.C. Block, J. Nucl. Sci. Tech. 15 (1978) 637.
[16] C. Guerrero, et al., Application of photon strength functions to (n, γ) measurements with the n_TOF TAC, in: Proceedings of the Workshop on Photon Strength Functions and Related Topics, June 17–20, 2007, Prague, CZ, PoS(PSF07)006.
[17] The n_TOF Collaboration, Measurement of the neutron capture cross-sections of ^{233}U, ^{240,242}Pu, ^{241,243}Am and ^{245}Cm with a Total Absorption Calorimeter at n_TOF, INTC-2003-036, 2003.
[18] M. Koizumi, et al., Nucl. Instr. and Meth. A 562 (2006) 767.
[19] O. Scherbakov, K. Furutaka, S. Nakamura, H. Harada, K. Kobayashi, Nucl. Instr. and Meth. A 517 (2004) 269.
[20] D.P. Barry, M.J. Trbovich, Y. Danon, R.C. Block, R.E. Slovacek, Nucl. Sci. Eng. 153 (2006) 8.
[21] R. Reifarth, et al., Nucl. Instr. and Meth. B 241 (2005) 176.
[22] S. Marrone, et al., Nucl. Instr. and Meth. A 517 (2004) 389.
[23] L. Tassan-Got, et al., Fission of actinides induced by neutrons at n_TOF, in: AIP Conference Proceedings on Nuclear Data for Science and Technology, vol. 769, AIP, Melville, 2004, p. 1529.
[24] M. Calviani, et al., Measurement of neutron induced fission of ^{235}U, ^{233}U and ^{245}Cm with the FIC detector at the CERN n_TOF facility, in: Proceedings of the International Conference on Nuclear Data for Science and Technology, vol. 750, Nice, France, 2007.
[25] R. Plag, et al., Nucl. Instr. and Meth. A 496 (2003) 425.
[26] F. Gunsing, et al., Nucl. Instr. and Meth. B 261 (2007) 925.
[27] K. Wisshak, et al., Nucl. Instr. and Meth. A 292 (1990) 595.
[28] M. Heil, et al., The Total Absorption Calorimeter of the n_TOF Collaboration, CERN n_TOF Report (ID: 250), February 2005. Available online from: www.cern.ch/ntof⟩.
[29] I. Dillmann, et al., The neutron absorber for the n_TOF TAC, n_TOF Internal Note, 2004.
[30] D. Cano-Ott, et al., Monte Carlo simulation of the 4π Total Absorption Calorimeter at n_TOF, n_TOF Internal Report, 2003.
[31] U. Abbondanno, et al., Nucl. Instr. and Meth. A 538 (2005) 692.
[32] http://www.acqiris.com⟩.
[33] http://castor.web.cern.ch/castor⟩.
[34] E. Berthoumieux, Preliminary report on BaF$_2$ Total Absorption Calorimeter test measurement, Rap. Tech., CEA-Saclay/DAPNIA/SPhN, 2004.
[35] D. Cano-Ott, et al., The n_TOF Collaboration, Measurements at n_TOF of the neutron capture cross section of minor actinides relevant to the nuclear waste transmutation, in: International Conference on Nuclear Data for Science and Technology, Santa Fe, USA, AIP Conference Proceedings,vol. 769, 2005, p. 1442.
[36] C. Guerrero, et al., A Monte Carlo based dead-time correction method for measurements in coincidence, to be submitted.
[37] C. Coceva, et al., Nucl. Instr. and Meth. A 489 (2002) 346.
[38] A. Mengoni, et al., The n_TOF Collaboration, The physics case and the related proposal for measurements at the CERN neutron time-of-flight facility n_TOF in the period 2006–2010 (the n_TOF phase-2 initiative), CERN-INTC-2005-021, 2005.
[39] R. Macklin, J. Halperin, R. Winters, Nucl. Instr. and Meth. A 164 (1979) 213.
[40] C. Domingo, et al., Phys. Rev. C 75 (2007) 015806.
[41] N.M. Larson, Updated users' guide for SAMMY: multilevel R-matrix fits to neutron data using Bayes' equations, ORNL/TM-9179/R6, 2003.
[42] The Joint Evaluated Fission and Fusion File (JEFF-3.1) http://www.nea.fr/html/dbdata/JEFF/⟩.
[43] J. Pancin, et al., Nucl. Instr. and Meth. A 524 (2004) 102.
[44] S.F. Mughabghab, Neutron Cross Sections, Academic Press, New York, 1984.
[45] C. Guerrero, et al., Measurement at n_TOF of the ^{237}Np(n, γ) and ^{240}Pu(n, γ) cross-sections for the transmutation of nuclear waste, in: Proceedings of PHYSOR-2006, ANS Topical Meeting on Reactor Physics. Vancouver, Canada. September 10–14, 2006.
[46] C. Guerrero, et al., Monte Carlo simulation of the n_TOF Total Absorption Calorimeter, to be submitted.
[47] P.E. Koehler, et al., Phys. Rev. C 62 (2000) 055803-1.
[48] M.C. Moxon, REFIT, A least square fitting program for resonance analysis of neutron transmission and capture data, Technical Report, AEA Industrial Technology, Harwell laboratory AEA-InTec-0470, 1991.
[49] B.J. Allen, A.R. Musgrove, R.L. Macklin, Neutron sensitivity of capture gamma ray detectors, in: Proceedings of a Specialists' Meeting on Neutron Data of Structural Materials for Fast Reactors, Geel, Belgium, 1977, pp. 506–529.
[50] K. Wisshak, et al., Phys. Rev. C 52 (1995) 2762.